Planetary and Space Science xxx (2017) 1–8

Contents lists available at ScienceDirect

Planetary and Space Science

journal homepage: www.elsevier.com/locate/pss

The mineralogy of newly formed dust in active galactic nuclei

Sundar Srinivasan [a,*], F. Kemper [a], Yeyan Zhou [b], Lei Hao [b], Sarah C. Gallagher [c,d], Jinyi Shangguan [e,f], Luis C. Ho [e,f], Yanxia Xie [e], Peter Scicluna [a], Sebastien Foucaud [h,g,a], Rita H.T. Peng [a,g]

[a] Institute of Astronomy & Astrophysics, Academia Sinica, 11F, Astronomy-Mathematics Building, No. 1, Roosevelt Rd, Sec 4, Taipei 10617, Taiwan, Republic of China
[b] Shanghai Astronomical Observatory, Chinese Academy of Sciences, 80 Nandan Road, Shanghai 200030, China
[c] Department of Physics and Astronomy, University of Western Ontario, London, ON N6A 3K7, Canada
[d] Centre for Planetary and Space Exploration, London, ON N6A 3K7, Canada
[e] Kavli Institute for Astronomy and Astrophysics, Peking University, Beijing 100871, China
[f] Department of Astronomy, School of Physics, Peking University, Beijing 100871, China
[g] Department of Earth Sciences, National Taiwan Normal University, Taipei 11677, Taiwan, Republic of China
[h] Center for Astronomy and Astrophysics, Shanghai Jiao Tong University, Shanghai 200340, China

ARTICLE INFO

Keywords:
Active galactic nuclei
Dust
Silicates

ABSTRACT

The tori around active galactic nuclei (AGN) are potential formation sites for large amounts of dust, and they may help resolve the so-called dust budget crisis at high redshift. We investigate the dust composition in 53 of the 87 Palomar Green (PG) quasars showing the 9.7 μm silicate feature in emission. By simultaneously fitting the mid-infrared spectroscopic features and the underlying continuum, we estimate the mass fraction in various amorphous and crystalline dust species. We find that the dust consists predominantly of alumina and amorphous silicates, with a small fraction in crystalline form. The mean crystallinity is 8±6%, with more than half of the crystallinities greater than 5%, well above the upper limit determined for the Galaxy. Higher values of crystallinity are found for higher oxide fractions and for more luminous sources.

1. Dust formation in active galactic nuclei

The observational appearance of quasars, particularly the obscuration of the central source, has been explained by the Unified Model, which invokes the presence of a dusty torus (*e.g.*, Antonucci, 1993; Bianchi et al., 2012; Netzer, 2015; Mason, 2015). Although initially envisioned as a static entity, the torus is now thought to be dynamic, and represents either an infalling gas (Hopkins et al., 2012) or an outflow of gas (*e.g.*, Königl and Kartje, 1994; Elitzur and Shlosman, 2006; Keating et al., 2012) with dust embedded in it. Silicates were proposed as the main constituent of this dust (Stenholm, 1994). Increasingly sophisticated radiative transfer models of the dusty tori predicted the appearance of both silicate absorption and emission, depending on the viewing angle (Pier and Krolik, 1992; Nenkova et al., 2002; van Bemmel and Dullemond, 2003; Hönig et al., 2006; Fritz et al., 2006; Stalevski et al., 2012), although initially only silicate absorption features were observed, indicative of a near edge-on viewing angle. The detection of silicate emission in active galactic nuclei (AGNs) is considered evidence for the unified model (Siebenmorgen et al., 2005; Hao et al., 2005; Sturm et al., 2005). In addition to the presence of silicates, other minerals have been predicted to condense as well, analogous to the dust formation sequence in evolved stars (Elvis et al., 2002). In principle, the exact condensation sequence, which can be probed by determining the dust composition, reveals information about the physical conditions in the dust forming (or processing) environments. Nevertheless, most infrared spectroscopic studies have focussed on measuring the optical depth in the silicate emission or absorption feature, using it as a proxy for the column density along the line-of-sight (e.g Shi et al., 2006; Hao et al., 2007; Sales et al., 2011; Hatziminaoglou et al., 2015). Some studies have even spatially explored variations in the column density, with particular emphasis on the nearby AGN NGC 1068 (*e.g.* Rhee and Larkin, 2006; Mason et al., 2006; Poncelet et al., 2006; López-Gonzaga et al., 2014; Alonso-Herrero et al., 2016; Lopez-Rodriguez et al., 2016), using standard astronomical silicate opacities such as those published by Draine and Li (2007). While

* Corresponding author.
E-mail addresses: sundar@asiaa.sinica.edu.tw (S. Srinivasan), ciska@asiaa.sinica.edu.tw (F. Kemper), 201111161006@mail.bnu.edu.cn (Y. Zhou), haol@shao.ac.cn (L. Hao), sgalla4@uwo.ca (S.C. Gallagher), shangguan@pku.edu.cn (J. Shangguan), lho.pku@gmail.com (L.C. Ho), yanxia.ts@gmail.com (Y. Xie), peterscicluna@asiaa.sinica.edu.tw (P. Scicluna), sebitosecos@gmail.com (S. Foucaud), htpeng1108@gmail.com (R.H.T. Peng).

http://dx.doi.org/10.1016/j.pss.2017.08.012
Received 12 December 2016; Received in revised form 28 March 2017; Accepted 25 August 2017
Available online xxxx

Table 1
The sample studied in this paper. The PG name and SIMBAD name are shown in the first two columns, followed by the positions. The redshifts are from Boroson and Green (1992). Absolute *B* magnitudes are taken from Schmidt and Green (1983). The last two columns are the host-corrected black hole masses and Eddington ratios from Ge et al. (2016). Table 1 is published in its entirety in machine-readable format. The first five rows are shown here for guidance regarding its form and content.

PG name	SIMBAD	RA	Dec	z	$M_{B,abs}$	$\frac{M_{BH}^{corr}}{M_\odot}$ (log)	$\frac{L_{bol}}{L_{Edd}}$ (log)
0003 + 158	PG 0003 + 158	0 5 59.24	16 9 49.0	0.451	−26.38	9.27	−0.388
0003 + 199	MRK 0335	0 6 19.58	20 12 10.6	0.0260	−22.14	7.15	−0.566
0007 + 106	MRK 1501	0 10 31.01	10 58 29.5	0.0890	−22.56	8.69	−1.09
0026 + 129	PG 0026 + 129	0 29 13.70	13 16 3.89	0.142	−24.76	8.59	−0.818
0043 + 039	PG 0043 + 039	0 45 47.23	4 10 23.4	0.385	−26.09	9.13	−0.722

Table 2
Details of the dust species used in this study. For each grain species, we compute the *Q* values assuming CDE with a volume corresponding to a spherical grain of 0.1 μm. The PAH emission is fit with an average interstellar profile. The material densities are taken from Klein and Dutrow (2008).

Species	Grain density (g cm^{-3})	Optical constants
Amorphous		
Corundum	4.02	Begemann et al. (1997)
Periclase	3.56	Hofmeister et al. (2003)
Olivine	3.79	Dorschner et al. (1995)
Mg-rich olivine	3.22	Jäger et al. (2003)
Crystalline		
Forsterite	3.2	Jaeger et al. (1998)
Clinoenstatite	3.28	Jaeger et al. (1998)
PAHs	–	Hony et al. (2001)

it was already reported by Sturm et al. (2005) that the silicates seen towards quasars differ from the Galactic interstellar silicates observed toward the Galactic Centre (*e.g.*, Kemper et al., 2004), only a handful studies have since attempted to explain the difference in spectral appearance in a relatively small number of objects, using a different dust composition (Jaffe et al., 2004; Markwick-Kemper et al., 2007; Köhler and Li, 2010), variations in the silicate mineralogy (Xie et al., 2014, 2015), different grain properties (Li et al., 2008; Smith et al., 2010) or optical depth effects (Nikutta et al., 2009). In this paper, we present the first results of a systematic study of AGN dust mineralogy by fitting the mid-infrared spectrum of a sample of Palomar Green (PG) quasars showing silicate emission following the method described by Markwick-Kemper et al. (2007), and trying to correlate the results with the physical properties of the AGN. We describe our sample selection in Section 2, and our model and fitting procedure in Section 3. We show our results in Section 4 and discuss the implications of these results in Section 5.

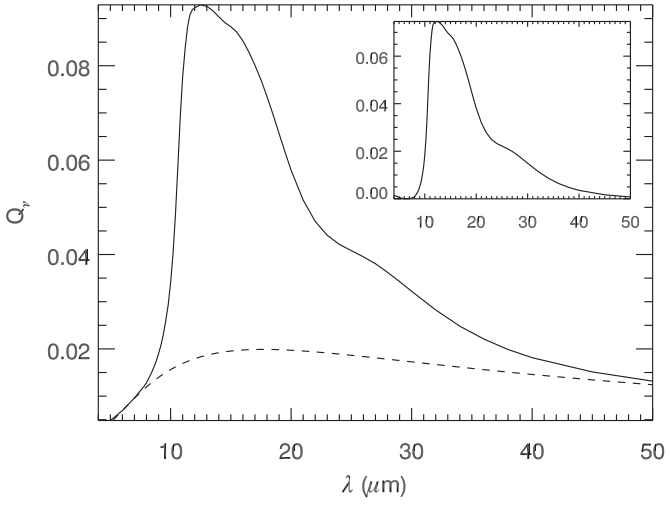

Fig. 1. The absorption efficiency Q_ν for corundum, with a robust polynomial fit (dashed line) to represent the underlying continuum, which is be used to compute the continuum-subtracted Q_ν (*inset*).

2. Sample selection

We derive our sample from the 87 nearby ($z \leq 0.5$) optically selected luminous broad-line QSOs in the Palomar Bright Quasar Survey (BQS) Catalog (Schmidt and Green, 1983; hereafter, the Palomar-Green or PG sample). These low-redshift objects were famously studied by Boroson and Green (1992), combining data at X-ray, optical, and radio wavelengths. More recently, the mid-infrared spectroscopic features of these objects (in particular, the strength of the 9.7 μm silicate emission) were studied by Shi et al. (2006) and Hatziminaoglou et al. (2015). Shi et al. (2014) obtained *Spitzer* photometry and spectroscopy for the entire PG sample. Petric et al. (2015) combined near-, mid-, and far-infrared information and computed the rest-frame luminosity and cold dust content for 85 of these 87 quasars.

Inclusion in the sample discussed by Petric et al. (2015) ensures a *Herschel* PACS 70 μm photometric measurement, which is essential to estimate the continuum emission longward of the 18 μm feature. Shi et al. (2014) also provide MIPS 70 μm photometry which can be used for the same purpose. By carefully re-reducing the Petric et al. (2015) *Herschel* data, Shangguan et al. (*in prep.*) derive lower 70 μm fluxes (15% lower on average). In this paper, we use the Shangguan et al. determinations for the 85 PG quasars studied by Petric et al. (2015). For the two remaining objects, we use the MIPS 70 data from Shi et al. (2014). This is reasonable, as the MIPS fluxes are in general agreement with the PACS values.

For each source in the PG sample, we obtained archival spectra from the *Combined Atlas of Sources with Spitzer IRS Spectra*[1] (CASSIS; Lebouteiller et al., 2011, 2015). For each source, we collect all available low-resolution spectra from the CASSIS database. If more than one observation exists for each module (short-low, 5–14 μm, and long-low, 14–40 μm), we average these observations. We then account for any mismatch between the short-low and long-low modules by scaling the former to the latter. Finally, we scale the synthetic photometry in the MIPS 24 band computed for each spectrum to the MIPS 24 flux as measured by Shi et al. (2014).

The spectra show a great variety in appearance, and many of them were included in the Spitzer Quasar and ULIRG Evolution Study (QUEST; Schweitzer et al., 2006; Netzer et al., 2007; Veilleux et al., 2009), where their spectral features and long-wavelength emission were discussed in detail. We briefly describe some common properties of the spectra here. Many of the spectra show emission features due to polycyclic aromatic hydrocarbons (PAHs) at rest wavelengths of 6.2, 7.7, 8.6, 11.2, and 12.7 μm, probably associated with star formation activity in the host galaxy. Furthermore, the H_2 S (3) 9.65 μm line can often be seen, as well as atomic emission lines related to starburst activity, in the form of [ArII] 6.986 μm, [NeII] 12.81 μm, and [NeIII] 15.56 μm lines. The spectra also feature some high ionization-potential lines typically found in AGN, such as the 10.51 μm [SiIV], the [NeV] 14.32 μm and the [OV] 25.89 μm lines. The dust emission spectrum shows a range of appearances of the solid

[1] http://cassis.sirtf.com.